UNIVERSITEIT VAN PRETORIA
UNIVERSITY OF PRETORIA
YUNIBESITHI YA PRETORIA

Raman and photoluminescence spectroscopy from magnesium doped, as grown, hydrogen implanted and annealed GaN

by

Martin Koena Maremane

Submitted in partial fulfilment of the requirements for the degree Masters of Science

in the

Faculty of Natural & Agricultural Science
(Department of Physics)
University of Pretoria
Pretoria
October 11, 2002

Supervisor: Prof H W Kunert
Co-supervisor: Prof F D Auret

© University of Pretoria

Summary

The presence of the hydrogen complex in Mg-doped GaN poses serious threats for the technological development of blue and ultraviolet light- emitting diodes and lasers. Since hydrogen is a difficult element to work with and it is incorporated into GaN through various mechanisms, a thorough understanding of hydrogen in GaN and other nitrides is essential to meet potential challenges by hydrogen.

Most of the work done on the interaction of hydrogen implanted Mg-doped GaN deals mainly with passivation of the dopants and formation of the hydrogen complex with magnesium. However, the role of hydrogen implantation on the optical properties of Mg-doped GaN is not well understood.

This study is mainly about optical properties of Mg-doped GaN and the effects of hydrogen on the Mg-doped GaN. Theoretically, group theory is used to determine the total number of symmetry allowed modes in GaN, Raman active modes and possible overtones. Experimentally, Raman and photoluminescence spectroscopy verify the theoretical results.

UNIVERSITEIT VAN PRETORIA
UNIVERSITY OF PRETORIA
YUNIBESITHI YA PRETORIA

Acknowledgements

I would like to thank the following persons for their help in this work:

- My supervisors, Prof. H. W. Kurnert and Prof. F. D. Auret who guided me through my study.
- Prof. D. J. Brink and Mrs L. Prinsloo, for helping me with PL and Raman measurements
- Mr M. J. Legodi, for the fruitful discussions we had and his encouragement.
- My dear mom who gave support since I was born and till now and my wife Pheladi and the children for being patient and encouraging throughout my study.
- The financial assistance of the University of Pretoria and National Research Foundation (NRF) is gratefully acknowledged.

Table of contents

1. Introduction 5
References 7

2. Experimental Procedure 8
2.1. Cleaning 8
2.2. Implantation 9
2.3. Photoluminescence 10
2.4. Photoluminescence system 11
2.5. Raman Scattering 12
2.6. Annealing 13
References 14

3. Theoretical Background 15
3.1. Electric dipole moment mechanism for one phonon scattering process 15
3.2. Determination of the possible vibrational modes in GaN with C^4_{6v} space group at $\mathbf{k} = 0$ of the Brillouin zone 16
3.3. Determination of all active Raman modes by means of group theory 22
References 24

4. Results and Discussion 25
4.1. Raman spectroscopy from as-grown Mg-doped GaN 25
4.2. Photoluminescence 30
4.3. The yellow band 34
4.4. The origin of the yellow band 36
References 38

5. Conclusion 40

Appendix 41

1. Introduction

It has been demonstrated that hydrogen in most semiconductors plays a pivotal role in determining the properties of semiconductors [1.1-1.6]. Nitrogen based semiconductors are of a huge interest because of their optical, electrical and mechanical properties [1.7]. Some of them possess a direct wide band gap and have high thermal stability. The main usage of nitrides is in application of blue/ ultraviolet (UV) light –emitting diodes and lasers, and high temperature electronics [1.8]. The success of the nitrides is partly dependent on an improved understanding and control of defect processes such as the hydrogen passivation. It also depends on how defects can be manipulated to achieve certain properties for the fabrication of devices.

Most of the GaN films are n-type auto- doped due to lack of suitable substrate that will match the lattice constant of GaN [1.9]. Another challenge was to get p-GaN conductivity, but it was dealt with successfully by post-growth treatment of the material to get rid of hydrogen complexes that might have been formed during growth [1.10].

Research on the role of hydrogen in semiconductors intensified in the 1980s, with the realization that hydrogen forms chemical complexes with shallow levels in semiconductors [1.11]. The ability of hydrogen to passivate and compensate both shallow and deep defects has a large influence on the electrical, mechanical and optical properties of several semiconductors [1.3]. However, further understanding of the properties of hydrogen in some semiconductors is required to deal with the challenges that may be caused by hydrogen and their technological implications, given the fact that hydrogen can be introduced in the material through various processes [1.12].

Hydrogen passivates p-type GaN and has little effect on n-type GaN. However, it was recently found that hydrogen also passivates some deep levels in n-type GaN [1.13]. Passivation in p-type GaN is characterized by a reduced hole concentration, decreased mobility and high resistivity.

Hydrogen is deliberately introduced in semiconductors through various mechanisms. Ion implantation or irradiation and plasma etching have proven to be the most used techniques. However, ion implantation creates damage to the sample. It allows control on the concentration, depth and lateral distribution of ions. It is mostly employed for device isolation in compound semiconductors. Annealing the sample helps to minimize the extent to which the damage can affect the sample. An interesting possibility would be to combine the passivation effects of hydrogen and the convenience of ion implantation to create regions in a semiconductor with varying p-type conductivities.

This study is based on the interaction of hydrogen with GaN. The effects of implanting p-type GaN with energetic hydrogen particles are established. Raman and photoluminescence spectroscopy are used to study the hydrogen implantation. To determine the number of possible and Raman active vibrational modes in hexagonal GaN, group theory is employed.

References

[1.1] H. P. Maruska and J. J. Tietjein, Appl. Phys. Lett. **15**, 327 (1969).

[1.2] S. C. Binari, H. B. Dietrich, G. Kelner, L. B. Rowland, K. Doverspike and D. K. Wickenden, J. Appl. Phys. **78**, 5, (1995).

[1.3] W. Gotz, N. M. Johnson, J. Walker, D. P. Bour, H. Amano and I. Akasaki, Appl. Phys. Lett. **67**, 18 (1996).

[1.4] H. Amano, M. Kito, K. Hiraamatsu and I. Akasaki, Jpn. J. Appl. Phys. **28**, L2112 (1989).

[1.5] S. Nakamura, M. Senoh, Y. Harada. Appl. Phys. Lett. **58**, 2021 (1991).

[1.6] M. Senthil Kumar, R Kesavamoorthy, P. Magudapathy, K. G. M. Nair and J. Kumar, Nucl. Instr. and Meth. In Phys. Res. B **179** (2001).

[1.7] Paul H. Holloway and Grary E. McGuire, in *Handbook of compound semiconductors Growth, Processing, Characterization, and Devices*, P68-72.

[1.8] S. Strite and H. Morkoç. J. Vac. Sci. Technol., B **10**, 1237 (1992).

[1.9] R, S. Averback and Mai Ghaly, Nucl. Instr. and Meth. in Phys. Res. B **127**, 128 (1997).

[1.10] J. W. Lee, S. J. Pearton, J. C. Zolper and R.A Stall. Appl. Phys. Lett. **68**, 2102,

[1.11] H. Morkoç, S. Strite, G. B. Gao, M. E. Lin, B. Sverdlov and M. Burns, J. Appl. Phys. **76,** 1363 (1994).

[1.12] A. Hierro, S. A. Ringel, M. Hansen, J Y. Okamoto, S. Hashiguchi, Y. Okada and M. Kawabe, Jnp. Appl. Phys. **38**, L230 (1999).

[1.13] S. Speck, U. K. Mishra and S. P. DenBaars, Appl. Phys. Lett., **77**, 10 (2000).

2. Experimental procedure

The Mg-doped GaN sample used in this work was grown with molecular beam epitaxy (MBE). The thickness of the Mg-doped GaN layer was 1-3 μm. The procedure followed in investigating the crystal structure and optical properties of hydrogen in Mg-doped samples is as follows:

- Clean the samples (five Mg-doped GaN samples were cut from one piece).
- Conduct Raman measurements on samples to establish the crystal structure of the samples.
- Implant the samples, except one sample that serves as a control, with hydrogen ions with Kaufman ion source.
- Perform Raman measurements on implanted samples to establish the effect of implantation.
- Characterize the samples using photoluminescence (PL) technique.
- Study the annealing kinetics of the implanted samples, using PL and Raman spectroscopy in Ar annealing.

2.1. Cleaning

The cleaning of samples involves three levels of surface treatment. The first (a, below) is designed to remove gross contamination, which is primarily hydrocarbon deposits. The second (b) removes particulate, metal atoms and contamination resulting from polishing residues and the third (c) etches and leaves the sample almost atomically clean [2.1].

All the GaN samples were cleaned with the following cleaning procedure:

a.i. Immerse in boiling trichloroethylene for 3 min.
ii. Immerse in boiling isopropanol for 3 min.
iii. Three rinses in H_2O for 20s each.

b.i. Immerse in boiling 3:1 HCl - HNO_3 for 8 -10 min.

ii: Three rinses in H_2O for 20s each.

c.i. Immerse in 1:1 HCl - H_2O for 3 min.

ii. Three rinses in H_2O for 20s each.

d. Dry in N_2 flow.

2.2. Implantation

The implantation of Mg-doped GaN samples took place at room temperature. The samples were implanted with hydrogen ions at angle 0^0, perpendicular to the surface of the samples, and the energy of ions was 26 keV. The dose of the implants ranged from 10^{12} to 10^{15} ions/cm^2. Before implantation could be executed, the depth profiles were calculated using the transport of ions in matter (Trim) programme [2.2]. The angle of this simulation calculation was 0^0.

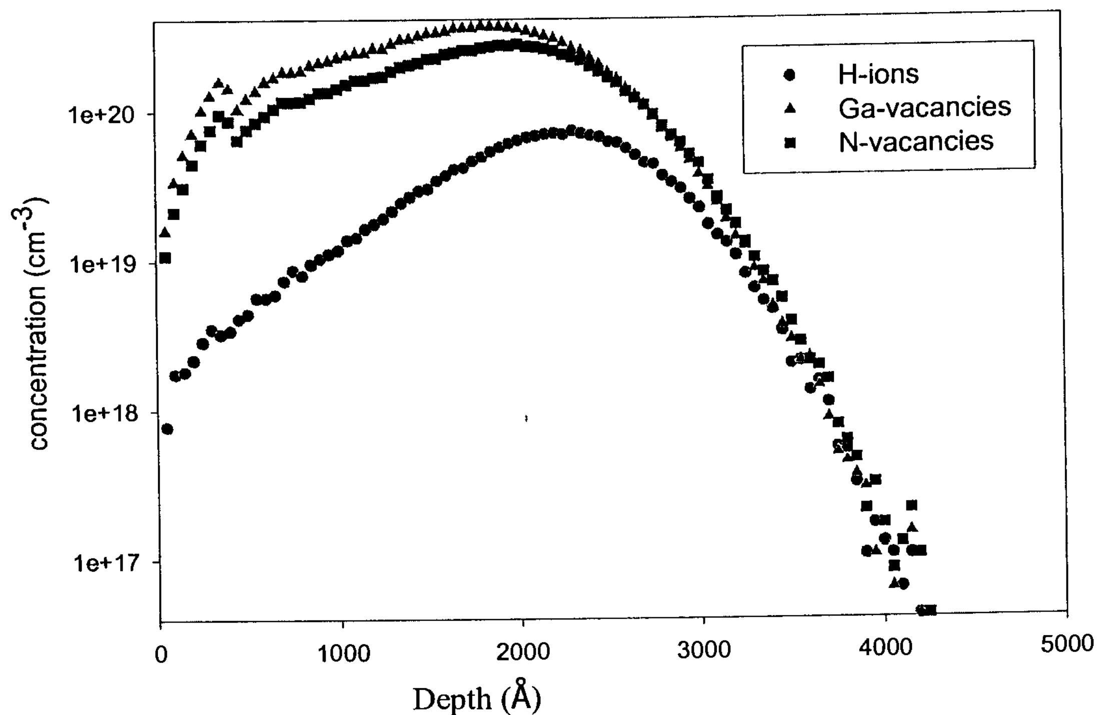

Figure 2.1. Trim calculation of hydrogen implanted in GaN at 26 KeV.

Figure 2.1 shows depth profile of 10^{15} cm^{-2} hydrogen in GaN calculated with Trim '98. The penetration depth or the range of hydrogen ions in GaN is approximately 0.43 μm. The maximum hydrogen concentration in the GaN is found within 0.23 μm, which makes it possible for further analysis with Raman and photoluminescence spectroscopy. Figure 2.1 also shows nitrogen and gallium vacancies created as a result of implantation.

2.3. Photoluminescence

PL yields information mainly about extrinsic optical properties [2.3]. An excitation of electron-hole pair (EHP) in the energy band gap of semiconductor can reveal different transitions. The presence of shallow levels in the energy band gap can be detected provided that these levels are radiative. Some deep levels can also be detected with PL if they are optical active as well.

PL is the study of luminescence emitted radiatively from a sample in the energy band gap by optical excitation source of energy greater than the band gap of the materials [2.4, 2.5]. This excitation results in the creation of electron-hole pairs (EHPs). Eventually, these EHPs combine because of recombination processes. Most of these processes are temperature dependent. Figure 2.2 demonstrates some of the recombination processes that take place in the energy band gap.

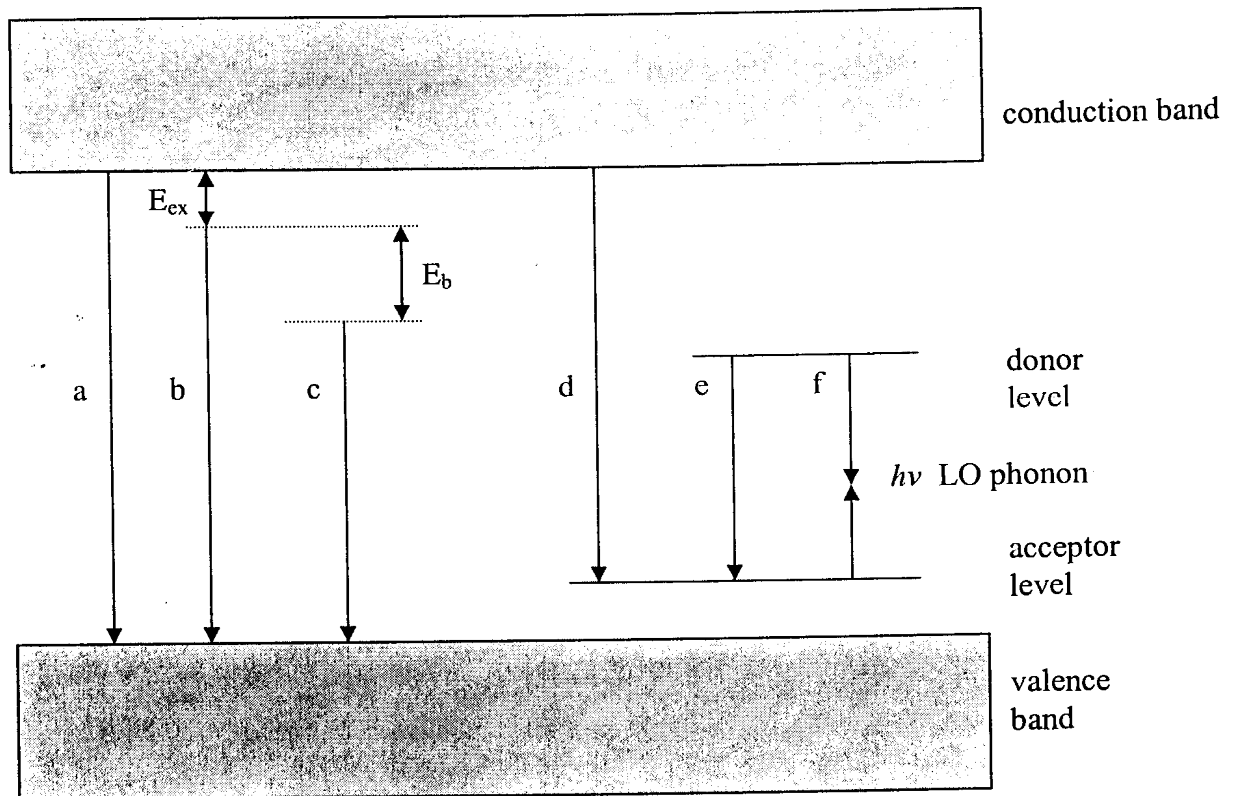

Figure 2.2. Different recombination processes taking place in semiconductors at room temperature, (a) band-to-band, (b) free exciton, (c) bound exciton, (d) free to bound, (e) bound-to-bound, and (f) longitudinal optical phonon.

2.4. Photoluminescence System

The PL system used in this study consists of a coherent 10 Watts max CW output Ar-laser that serves as excitation source. The output beam from the laser passes through a laser-line filter, which eliminates extraneous photon emissions, which are the result of plasma noise in the laser. The laser light is focused onto the sample as in figure 2.3. The luminescence signal emitted from the sample is collected by the lens and coupled into a monochromator. The output intensity or signal of the luminescence is dispersed by the monochromator and is detected by photomultiplier tube (PMT). The PMT amplifies the signal and produces direct current. This direct current is measured using

UNIVERSITEIT VAN PRETORIA
UNIVERSITY OF PRETORIA
YUNIBESITHI YA PRETORIA

an electrometer and is analyzed by a computer capable of quick retrieving, plotting and storing of data.

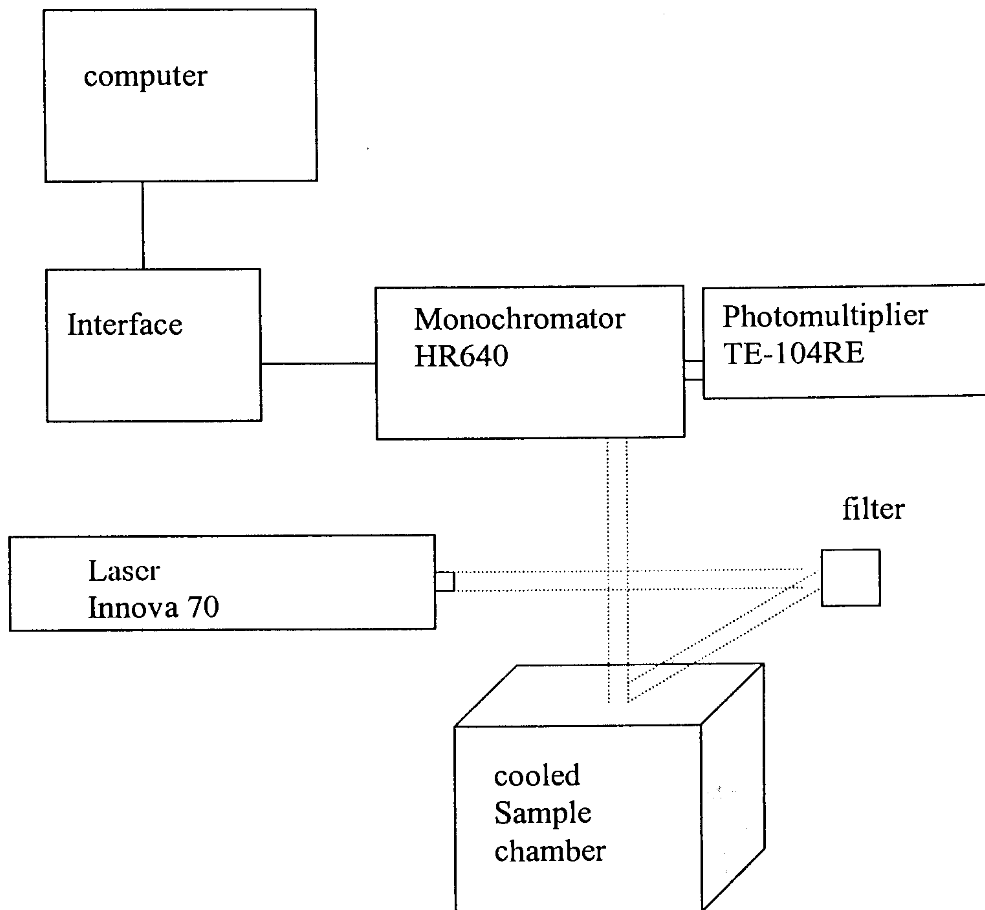

Figure 2.3. A schematic diagram of a simplified version of Photoluminescence system.

2.5. Raman scattering

Raman spectroscopy gives information about the crystalline quality and other important properties of semiconductor such vibrational modes and localized phonons. It is also very sensitive to ion implantation-induced defects and any irregularities in a crystal [2.7-2.9].

In the present study, Raman measurements were carried out at room temperature using the 514.5 nm line of an Ar^+ laser as an excitation source. The laser beam was focused by a microscope lens system yielding a spot of 1μm. The scattered light was detected in backscattering geometry using Dilor XY 800 mm triple-grating spectrometer with a liquid nitrogen cooled charge coupled detector. Raman signals from both substrate, implanted and unimplanted regions contribute to the Raman spectra since the penetration depth of the incident laser light is larger than the thickness of the GaN layers.

2.6. Annealing

After each PL measurement, samples were thermally annealed in a Lindeberg "hevi-duty" furnace from 200 to 900 ^{0}C, in steps of 100 ^{0}C for 1hour. The annealing process took place in an argon atmosphere to minimize the effect of oxidation on the surface of the samples. The temperature was monitored by placing a thermocouple inside the sample holder next to the samples.

References

[2.1] L. L Smith, S.W. King, R. J. Nemanich and R. F. David, Journal. of Electronic Material **25**, 567 (1996).

[2.2] R. Seitz, C. Gaspar, T. Monteiro, E. Pereira, M. Leroux, B. Beaumont, and P. Gibart, MRS Internet J. Nitride Semicond. Res. **2,** 36 (2001).

[2.3] J. P. Biersack and J. F. Ziegler, in *Ion Implantation Techniques*, Springer, Berlin (1982).

[2.4] D. J. Ashen, P. J. Dean, D. T. J. Hurle, J. B. Mullin, A. M. White, and P. D. Greene, J. Phys. Chem. Solids **36**, 1041 (1975).

[2.5] A. W. R. Leitch and H. L. Ehlers, Infrared Phys. **28**, 433 (1988).

[2.6] A. Lee-Smith, in *Applied Infrared Spectroscopy: Fundamentals, Techniques and Problem solving*, John Wiley and Son, New York (1979).

[2.7] T. Ruf, in *Phonon Raman Scattering in semiconductors, Quantum wells and superlattices*, Springer, (1998).

[2.8] D. K. Schroder, in *Semiconductor material and device characterization 2th*, John Willey and sons, (1998).

[2.9] Bill George and Peter McIntyre, in *Infrared Spectroscopy,* John Wiley and Son, (1999).

3. Theoretical background

In this section, the fundamental mechanism of Raman scattering provided by classical theory is discussed. The group theory is used to determine the total number of active modes in GaN.

3.1. Electric dipole moment mechanism for one Raman phonon scattering process.

A monochromatic incident light wave of frequency ω_0, time t and electric field

$$\mathbf{E} = \mathbf{E}_0 \cos \omega_0 t \tag{3.1}$$

induces in a crystal (or molecule) a dipole moment

$$\mathbf{P} = \alpha \mathbf{E} = \alpha \mathbf{E}_0 \cos \omega_0 t \tag{3.2}$$

where α is the polarizability tensor. If we resolve **P**, α and **E** in the x, y, and z directions, they can be written as

$$\begin{bmatrix} P_x \\ P_y \\ P_z \end{bmatrix} = \begin{bmatrix} \alpha_{xx} & \alpha_{xy} & \alpha_{xz} \\ \alpha_{yx} & \alpha_{yy} & \alpha_{yz} \\ \alpha_{zx} & \alpha_{zx} & \alpha_{zz} \end{bmatrix} \begin{bmatrix} E_{0x} \\ E_{0y} \\ E_{0z} \end{bmatrix} \cos \omega_0 t \tag{3.3}$$

The direction of the polarization does not coincide with the direction of the applied field because the direction of the chemical bonds in the crystal also affects the direction of polarization. If the crystal is vibrating with frequency ω, the nuclear displacement is written as

$$Q_j = Q_j^0 \cos \omega t , \tag{3.4}$$

where Q_j^0 is the vibrational amplitude.

The corresponding component of the oscillating electric moment is therefore given by the equation below [3.1],

$$\mathbf{P}_i = \mathbf{E}_{0i} \left[\alpha_i^0 \cos \omega_0 t + \sum_j \left(\frac{\partial \alpha_i}{\partial Q_j}\right)_0 Q_j^0 \left(\frac{1}{2} \cos(\omega_0 + \omega) + \frac{1}{2} \cos(\omega_0 - \omega) \right) \right] \tag{3.5}$$

where i and j are positive integers.

It is apparent that the light emitted by the induced oscillating dipole moment from a crystal will contain:

I. The shift frequency $\omega_0 \pm \omega$ and

II. The incident frequency ω_0

First order of Raman spectroscopy provides the experimental values of the frequency shift $\omega_0 \pm \omega$ demonstrated on figure 3.1. This approach is valid only for one -phonon process at k = 0 (point Γ of the Brillouin zone).

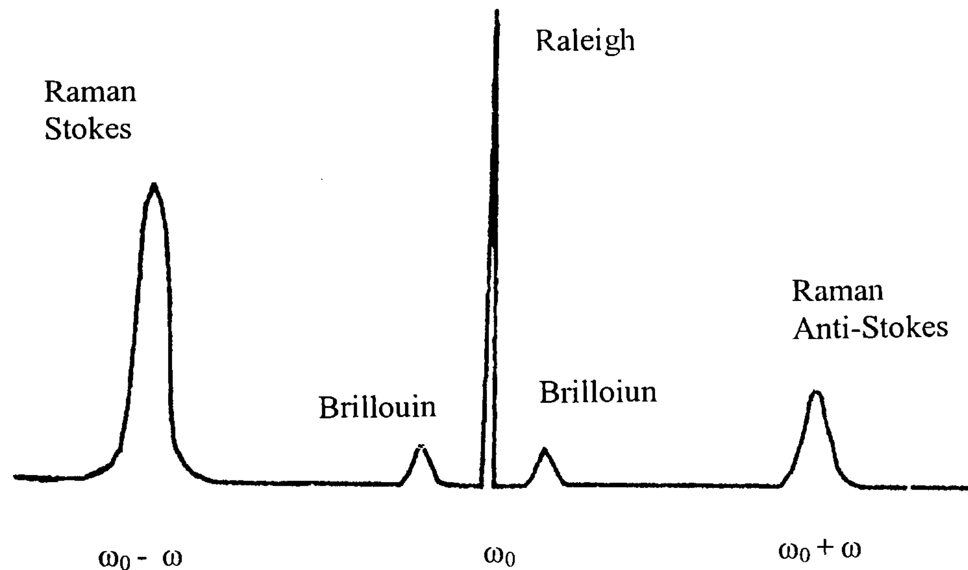

Figure 3.1. The energy distribution of various scattered light [3.2].

3.2. Determination of the possible vibrational modes in GaN with C^4_{6v} space group at k = 0 of the Brillouin zone.

In this section the total number of possible vibrational modes in a crystal is derived. The representation of the factor group C^4_{6v} /τ (τ is infinite translation space group) corresponding to atomic permutations (Ga and N) is derived. The reducible base containing 12 vectors is introduced, six displacements and six angles between the Ga and N atoms as shown in figure 3.2a and 3.2b. Imposing symmetry operations onto our base we generate the 12 x12 reducible representations that we decompose onto irreducible representation (irrps) of the point C^4_{6v} group. The irrps of the C^4_{6v}

contained in the 12 x 12 permutational representation fully determine the number of allowed modes and their symmetries in GaN at k = 0, as well as in all compounds with C^4_{6v} space group.

The C^4_{6v} space group at k = 0 consists of:

1. pure rotations
2. three screw rotations
3. three glide planes associated with non-primitive translation (τ) and three pure glide planes.

The figure 3.2a and 3.2b show the Ga (black) and N (grey) atoms arrangement in a crystal and symmetry operations of the $\bar{C}_{6v}$ group are indicated. The basis vectors transform onto each other due to the symmetry operations:

E, $(C_6^{\pm}/\tau)$, $(C_3^{\pm})$, (C_2/τ), δ_{v1}, δ_{v2}, δ_{v3}, (δ_{d1}/τ), (δ_{d2}/τ), (δ_{d1}/τ)

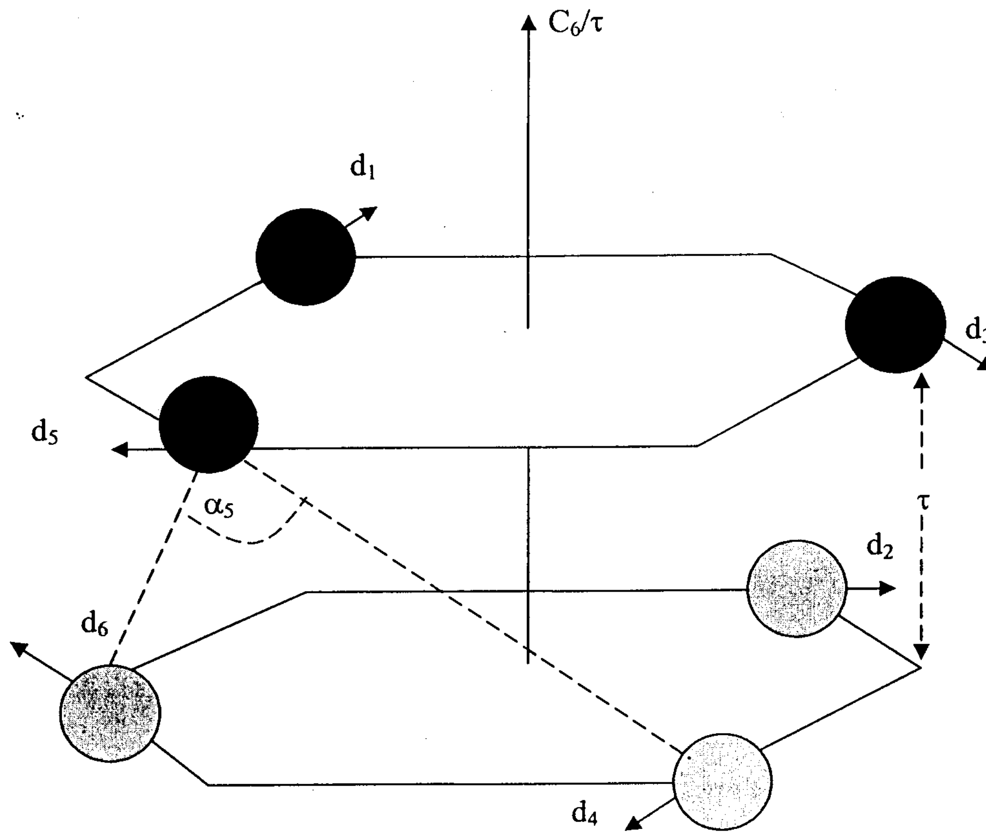

Figure 3.2a. Arrangement of the Ga and N atoms in GaN crystal.

α_5 is the angle between atom $d_4\, d_5\, d_6$ and α_1, α_2, α_3, α_4, and α_6 are the angles between atoms $d_6\, d_1\, d_2$, $d_1\, d_2\, d_3$, $d_2\, d_3\, d_4$, $d_3\, d_4\, d_5$ and $d_5\, d_6\, d_1$ respectively but they are not shown in the diagram.

UNIVERSITEIT VAN PRETORIA
UNIVERSITY OF PRETORIA
YUNIBESITHI YA PRETORIA

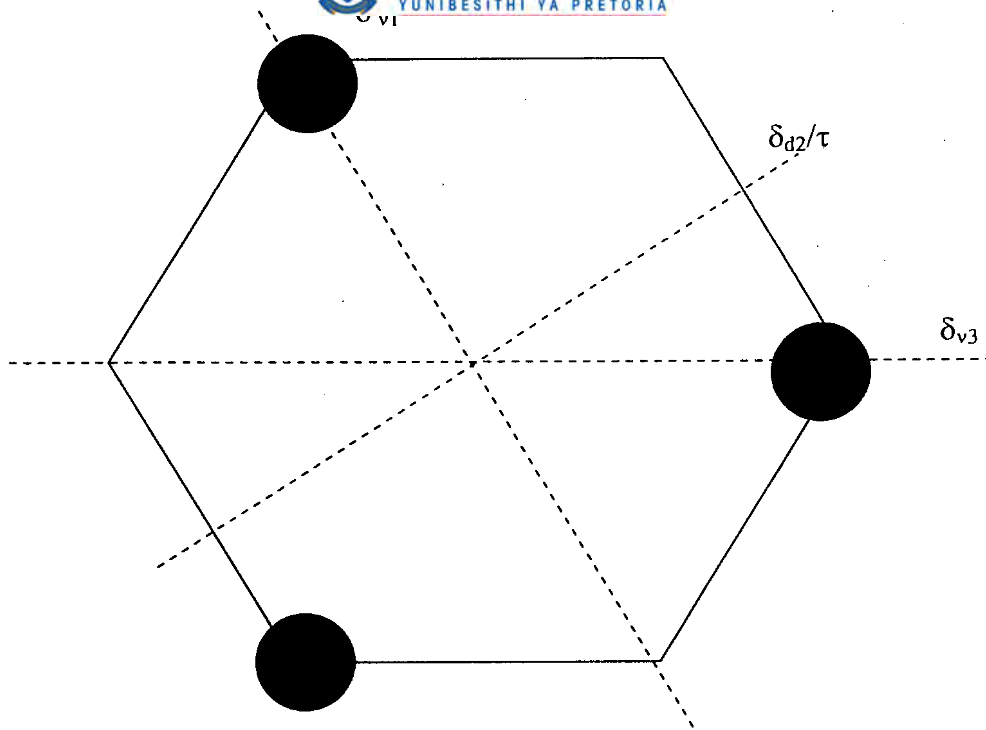

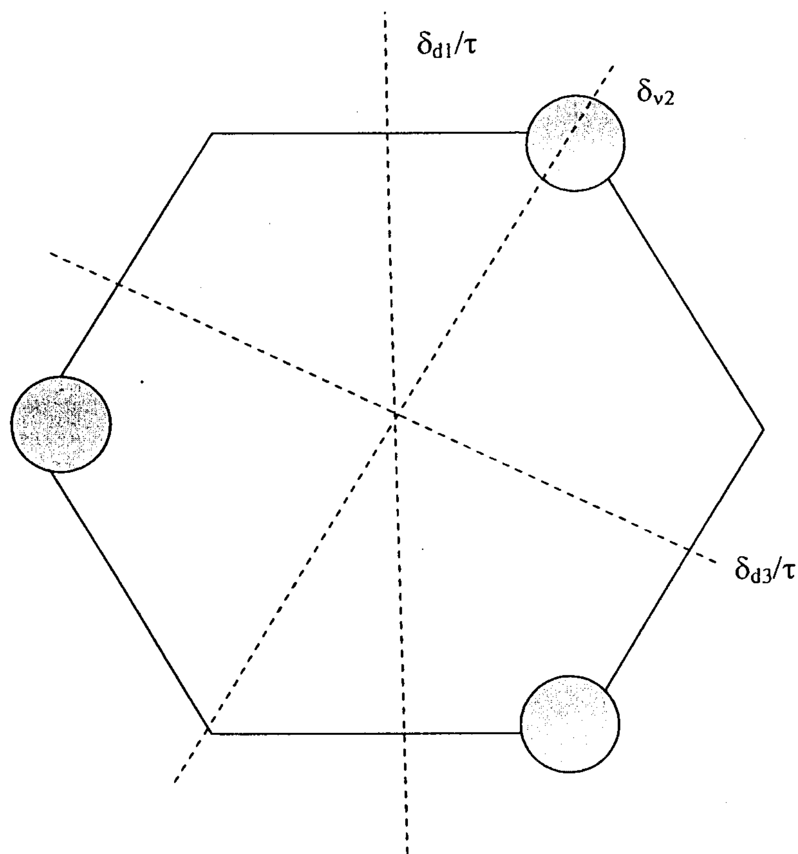

Figure 3.2b. Six symmetry operations in GaN.

The chosen basis vectors are the following;

- three displacement d_1, d_3 , d_5 from the equilibrium position (lattice) of Ga atoms lying on the upper plane,
- three displacement d_2 , d_4 , d_6 of the N atoms lying on the lower plane and
- the six angles α_i (i = 1 - 6) between bonds of the Ga and N atoms.

The symmetry operations of the $\bar{C}_{6v}$ group which involves non-primitive translation (τ), transform Ga and N atoms onto each other after screw rotations, $2(C_6/\tau)$, $2C_3$, (C_2/τ) and three reflections in diagonal planes $3(\delta_d/\tau)$ and glide plane $3\delta_v$. It should be noted that $\bar{C}_{6v}$ is not strictly speaking a point group C^4_{6v}, because it contains non-primitive translation τ. However, it is clear that these two groups, C^4_{6v} and $\bar{C}_{6v}$ are isomorphic because their irrps have the same characters listed in table 3.1.

In finding all possible symmetry modes of GaN, the CDML tables [3.3] are used. The detailed calculations are given in Appendix A. Since group $\bar{C}_{6v}$ consists of six classes, we have derived only matrices of the first symmetry operation in a class. We denote the "permutations" representations as D_{per}.

Table 3.1. The characters of the irreducible representation of the permutation of the C^4_{6v} group and the reducible displacement representation D_{per} [3.3-3.4].

CDML	Koster	Bethe	E	$2(C_6/\tau)$	$2C_3$	(C_2/τ)	$3\delta_v$	$3(\delta_d/\tau)$
D_{per}			12	0	0	0	4	0
Γ_1	A_1	Γ_1	1	1	1	1	1	1
Γ_2	A_2	Γ_2	1	1	1	1	-1	-1
Γ_3	B_1	Γ_3	1	-1	1	-1	-1	1
Γ_4	B_2	Γ_4	1	-1	1	-1	1	-1
Γ_5	E_1	Γ_5	2	-1	-1	2	0	0
Γ_6	E_2	Γ_6	2	1	-1	-2	0	0
$A_1 \oplus E_2$			3	2	0	-1	1	1

Using the reduction equation (3.1),

$$\mu_{ri} = \frac{1}{g}\sum \chi^D\left(g/\tau_g\right).\chi^{ri(*)}\left(g/\tau_g\right).g_i \tag{3.6}$$

where g is the number of the elements in the group, $\chi^D\left(g/\tau_g\right)$ is the characters of D_{per}, $\chi^{ri(*)}\left(g/\tau_g\right)$ is the characters of the vibration species and g_i is the number of classes.

The 12 x 12 reducible representations D_{per} is decomposed into irreducible representation of the $\bar{C}_{6v}$ group (CDML). Clearly only eight modes can be realized in hexagonal crystal with C^4_{6v} space group and these are contained in our permutational representation

i 17388247
b16370429

$$D_{per} = 2A_1 \oplus 2B_2 \oplus 2E_1 \oplus 2E_2 \qquad (3.7)$$

3.3. Determination of all active Raman modes by means of group theory.

In order to determine the Raman active modes in hexagonal crystals with the C^4_{6v} space group we decompose the Kronecker product (KP) of its vector representation $D^v \otimes D^v$ onto irrps. Since the Raman tensor is symmetric, we split the KP into symmetrized and antisymmetrized parts. Only the irreducible representation contained in the symmetrized KP will be Raman active [3.6].
In the C^4_{6v} group the vector representation is

$$D^v = A_1 \oplus E_2 \qquad (3.8)$$

The KP becomes:

$$D^v \otimes D^v = (A_1 \oplus E_2) \otimes (A_1 \oplus E_2)$$

$$= \begin{bmatrix} A_1 & 0 \\ 0 & E_2 \end{bmatrix} \otimes \begin{bmatrix} A_1 & 0 \\ 0 & E_2 \end{bmatrix}$$

$$= 2A_1 \oplus 2E_1 \oplus 2E_2 \oplus \{A_2\}_{ansym} \qquad (3.9)$$

Therefore, only the six irreducible modes $2A_1$, $2E_1$ and $2E_2$ are Raman active in the crystal with C^4_{6v} space group.

The result can be verified by means of the equations

$$\left[\chi^{(m)}(R)\right]^{sym}_{(2)} = \frac{1}{2}\left[\left(\chi^{(m)}(R)\right)^2 + \chi^{(m)}\left(R^2\right)\right] \qquad (3.10a)$$

$$\left[\chi^{(m)}(R)\right]^{ansym}_{(2)} = \frac{1}{2}\left[\left(\chi^{(m)}(R)\right)^2 - \chi^{(m)}\left(R^2\right)\right] \qquad (3.10b)$$

with R ≡ {g/τg}, m is representations in table 3.1.

The knowledge of Raman active modes in GaN will help us to identify "induced" new modes by doping implantation, annealing and other kind of treatments. The frequencies of the Raman modes in GaN have been determined by several authors and they are listed in table 3.2.

Table 3.2. Raman active modes in GaN

Phonon mode	E_2 (low)	A_1 (TO)	E_1 (TO)	E_2 (high)	A_1 (LO)	E_1 (LO)
Frequency (cm^{-1})	144	531	557	567.3	735	742
Energy (meV)	17.9	65.8	69.1	70.3	91.1	92

References

[3.1] T. Ruf, in *Phonon Raman Scattering in semiconductors, Quantum wells and superlattices*, Springer, (1998).

[3.2] M. Hamermesh, *in Group Theory and its Application to Physical Problems*, Pergamon Press Oxford London, New York and Paris. Adison-Wesley Publishing Company, Inc. 1962.

[3.3] P. Cracknell, B. L. Davies, S. C. Miller, W. F. Love, Kronecker Product Tables, Vol. 1-4, (1F1/Plenum, New York, Washington, London , 1979)

[3.4] G. F. Koster, *in Space Group and their respresentation (academicpress)*, New York 1975.

[3.5] L. E. McNeil, *in Properties of Group III Nitrides*, Edited by James H. Edgar, Kansas State University, USA, EMIS Data reviews Series No. **11**, (1994).

[3.6] H. W. Kunert, submitted to "applied surface science"

4. Results and discussion

In this chapter, the results obtained from Raman and photoluminescence spectroscopy to determine the effect of hydrogen in Mg-doped GaN are mentioned and discussed. The Raman results accord with the predicted number of phonons as determined in the previous chapter. The luminescence bands observed by Raman prompted a full analysis by making use of photoluminescence spectroscopy. However, this study reveals that Raman and photoluminescence spectroscopy complement each other. Finally in this chapter, thorough attention is paid to the origin of the yellow band as observed after annealing.

4.1. Raman spectroscopy from as-grown Mg-doped GaN

Most of GaN samples are transparent to incident laser beam, so it is possible to analyse the entire region of the GaN and the substrate. Samples used in this study have a hexagonal structure, which belong to C^4_{6v} space group with six atoms in the unit cell. At k = 0, the group theory predicts six Raman active modes (see chapter 3). One set of the A_1 and one set E_1 correspond to acoustic phonons and B_1 modes are silent [4.1]. Due to longitudinal and transverse optical modes splitting, GaN has six Raman-active optical modes namely, A_1 (TO), E_1 (TO), A_1 (LO), E_1 (LO), E_2 (low) and E_2 (high).

Figure 4.1a, b display Raman spectra measured from as-received Mg-doped GaN and hydrogen implanted and annealed Mg-doped GaN. In the as-received sample, four of the six active Raman modes are present: A_1(TO)-534, E_1(TO)-560, E_2(high)-570, A_1(LO)-735.4 cm^{-1}. In addition, on the low energy side of the spectrum, the modes at 320 and 380 cm^{-1} are observed, these can not be assigned to the Raman active E_2(low)-17.9 meV and E_1(LO)-92 meV because normally they are not observed by ordinary Raman spectroscopy. However, they can be observed by polarization techniques, X-rays spectroscopy or neutron scattering spectroscopy. Nevertheless, the 320 cm^{-1} mode (40 meV) can be associated with the presence of a low energy acoustic phonon calculated and measured by time-of-flight neutron spectroscopy by Nipko et al [4.2]. However, the authors did not assign the symmetries to their measured and calculated phonons.

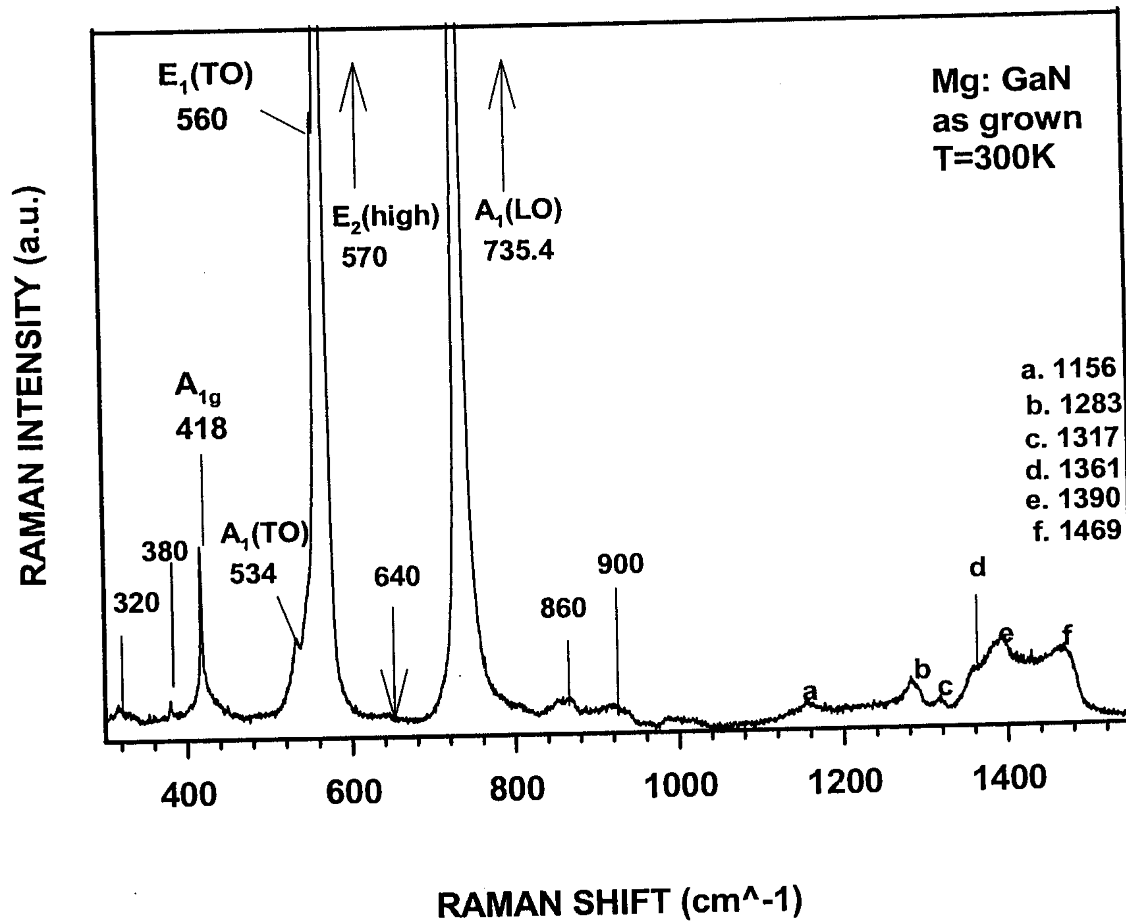

Figure 4.1a. Raman spectra for as-received Mg-doped GaN, recorded at 300K.

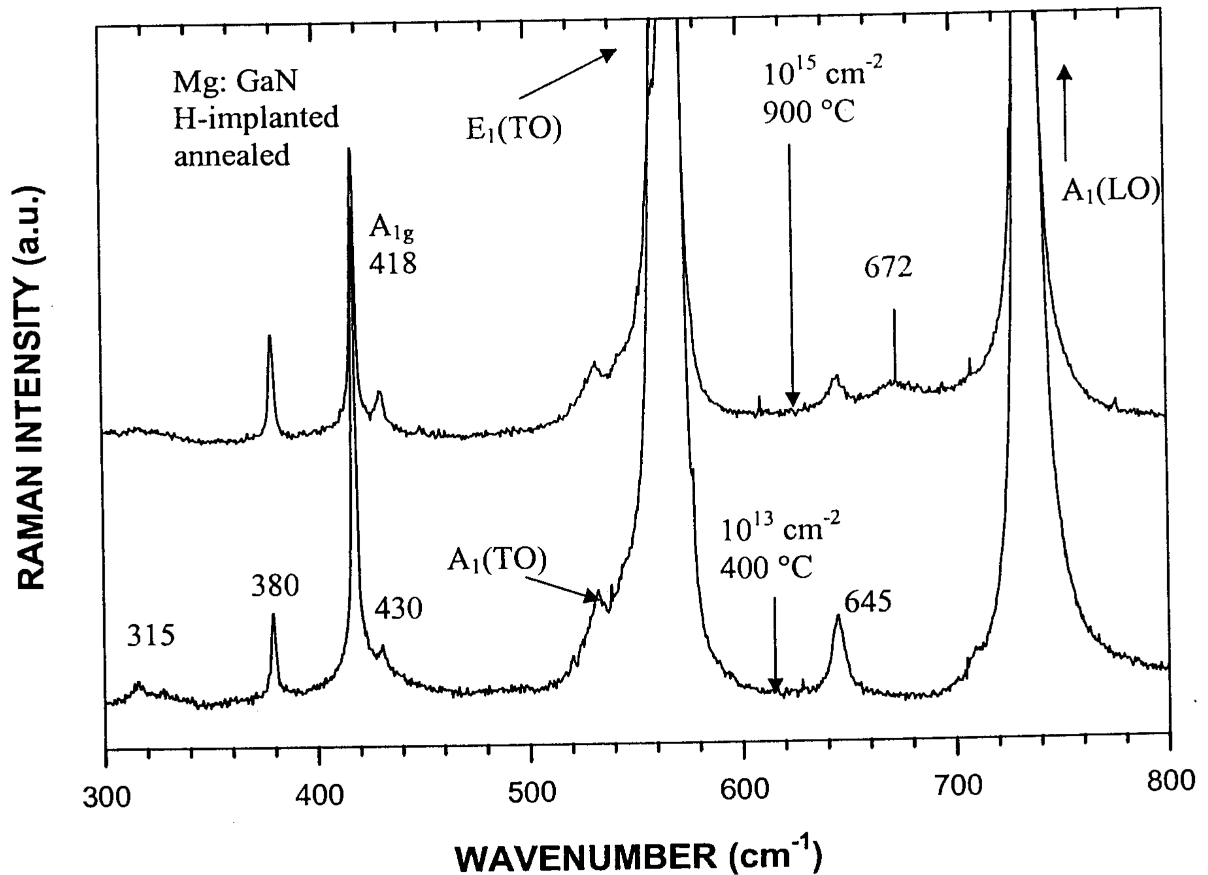

Figure 4.1b. Raman spectra for implanted and annealed Mg-doped GaN.

In chapter 3 we classify the eight phonon states according to their irreducible representations, these follow from the space group C^4_{6v} at **k** = 0 of the GaN. The mode at 640 cm^{-1} is Mg related and has already been reported [4.3]. Hydrogen implantation at moderate dose, 10^{13} cm^{-2}, and moderate annealing temperature, 400 °C, reveals a new mode at 430 cm^{-1} and enhances essentially the 380 and 645 cm^{-1} modes. At higher dose, 10^{15} cm^{-2}, and 900 °C annealing temperature another new vibrational state appears at 672 cm^{-1}. The second order phonons are depicted on figure 4.1a, there are several second order modes showing a considerable phonon density of states (DOS). Three of them have been discussed previously [4.4, 4.5]. The mode at 1470 cm^{-1} is exactly twice the energy of the first order zone-centre, A_1(LO) phonon. We attribute it to overtone scattering due to two phonons of the corresponding branch near the centre of the Brillouin zone (BZ). In the region 4200-4900 cm^{-1} of the Raman shift several broad luminescence bands at 1.878, 1.85, 1.836, and 1.8eV are present as shown on figure 4.2. Raman spectra taken in the region 4900–5100 cm^{-1}, presented on

figure 4.3, exhibit two well resolved luminescence bands centred at wavelength shifts 5006 and 5035 cm^{-1}, respectively. The luminescence bands closely resemble well known "doublet"- transitions originating from the Cr^{+3} in sapphire [4.6].

To verify our hypothesis we have taken the low temperature photoluminescence spectra showed in figure 4.7. Indeed, three well resolved transitions centred at 1.737, 1.785 and 1.789 eV are present. All of them have been previously observed [4.7]. The fact that the intensities of the R_1 and R_2 transitions [4.7] are implantation dose dependent would suggest that the implanted hydrogen ions reached the sapphire substrate and they are possibly involved with the Cr^{+3} complexes or Cr^{+3} complexes were formed during growing process.

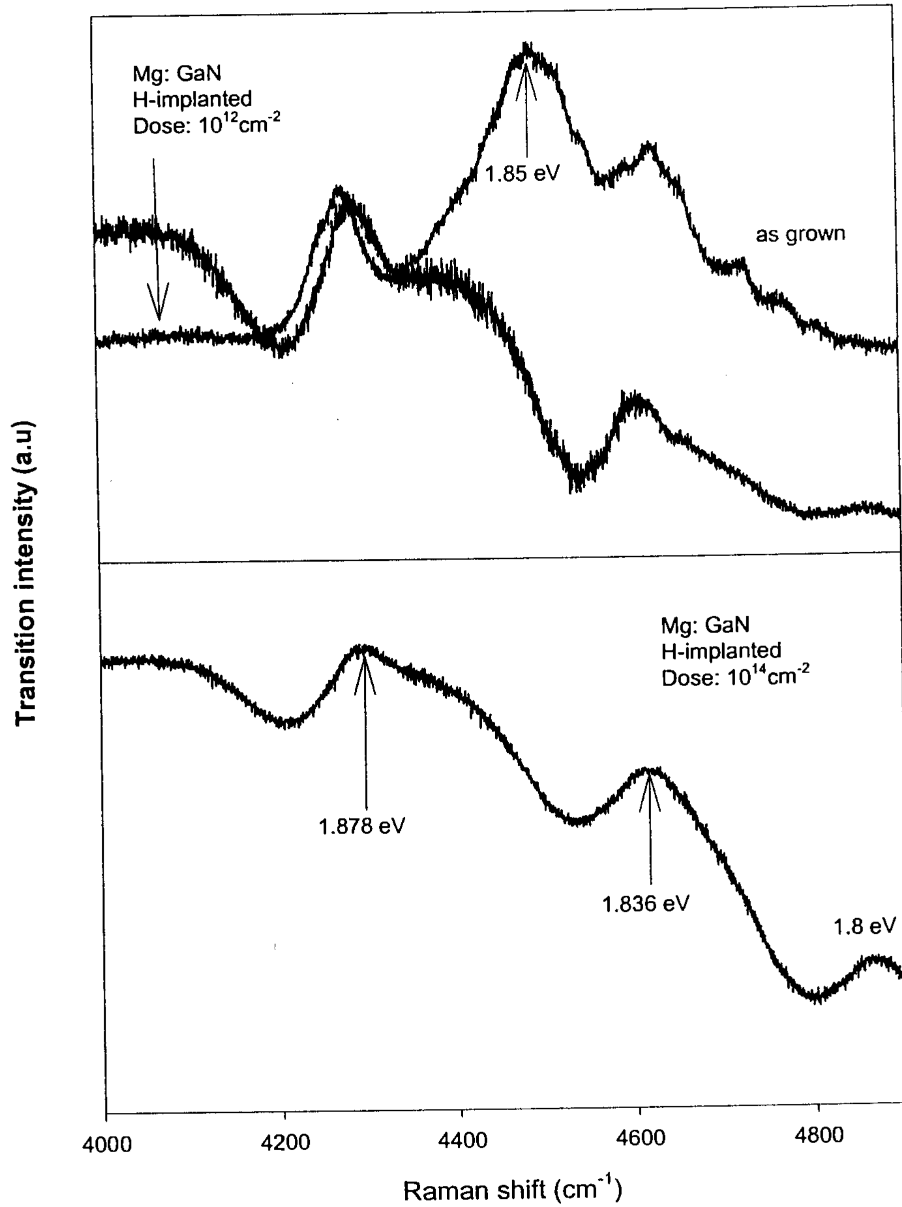

Figure 4.2. Raman shift showing broad luminescence bands at 1.878, 1.85, 1.836, and 1.8eV Mg-doped GaN.

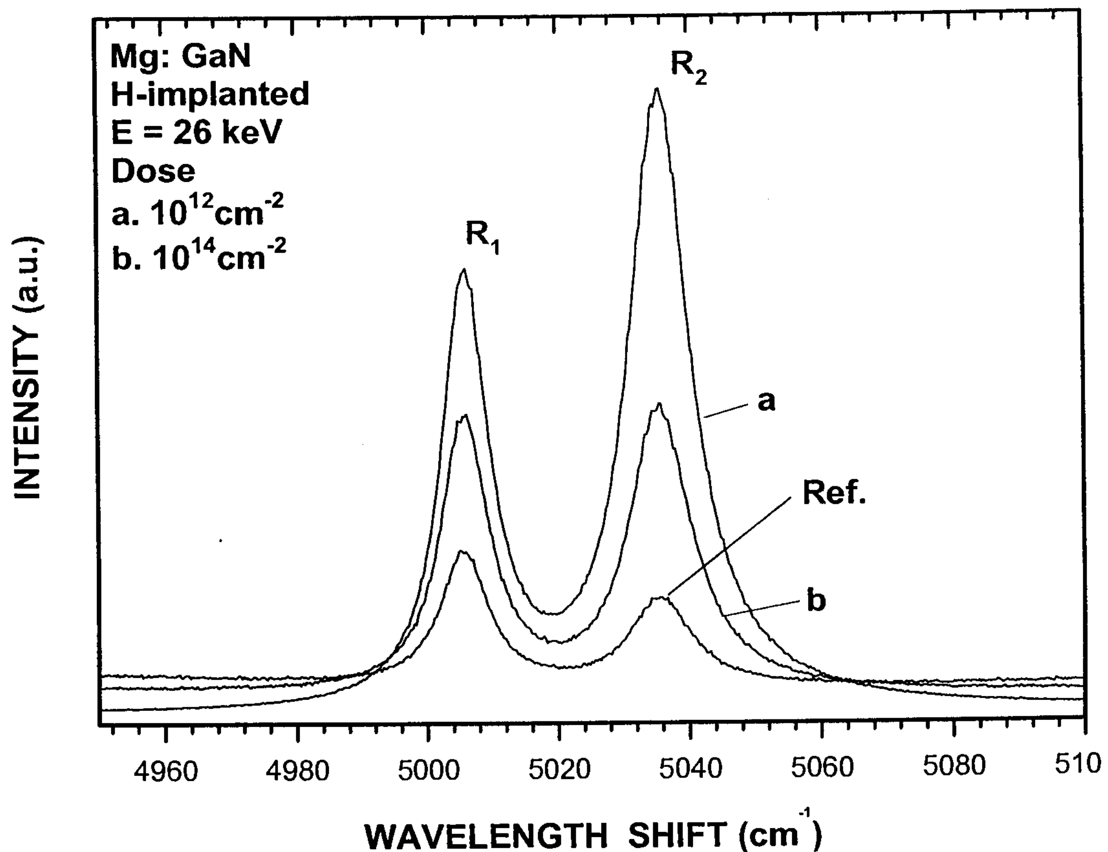

Figure 4.3. The doublet emission for Cr^{3+} in sapphire substrate monitored by Raman spectroscopy.

4.2. Photoluminescence

Figure 4.4 displays PL spectra taken from as grown Mg-doped GaN and implanted (dose 10^{12} cm^{-2}) and annealed samples. From the as grown sample a weakly resolved free-exciton (FX) transition at about 3.48 eV is observed, as well as several bands centered at: 3.28, 3.24, 3.20, 3.12, 3.08, 3.0, 2.92, 2.84, and 2.76 eV. The bands at 3.28 and 3.2eV are frequently associated with DAP's (shallow-donor to shallow acceptor Mg complexes). The low energy shoulders (3.24 and 3.12eV with substructures at about 40 meV energy spacing) have two possible origins: 1) They may belong to different electronic states of the DAP's or 2) they are simply phonon replicas. In the later case of the 40 meV energy phonon does not fit any of the six ($2A_1$, $2E_1$, and $2E_2$) Raman active modes. Nevertheless, it may be related to an acoustic mode of 40meV energy recently measured and calculated by Nipko et al

[4.2]. It should be pointed out that from the reference sample we do not observe any well resolved excitonic transitons and also see no trace of the YL band. This may be due to the fact that our Mg doping (about 10^{19} cm^{-3}) is to low to observe the YL band and to high to monitor excitons.

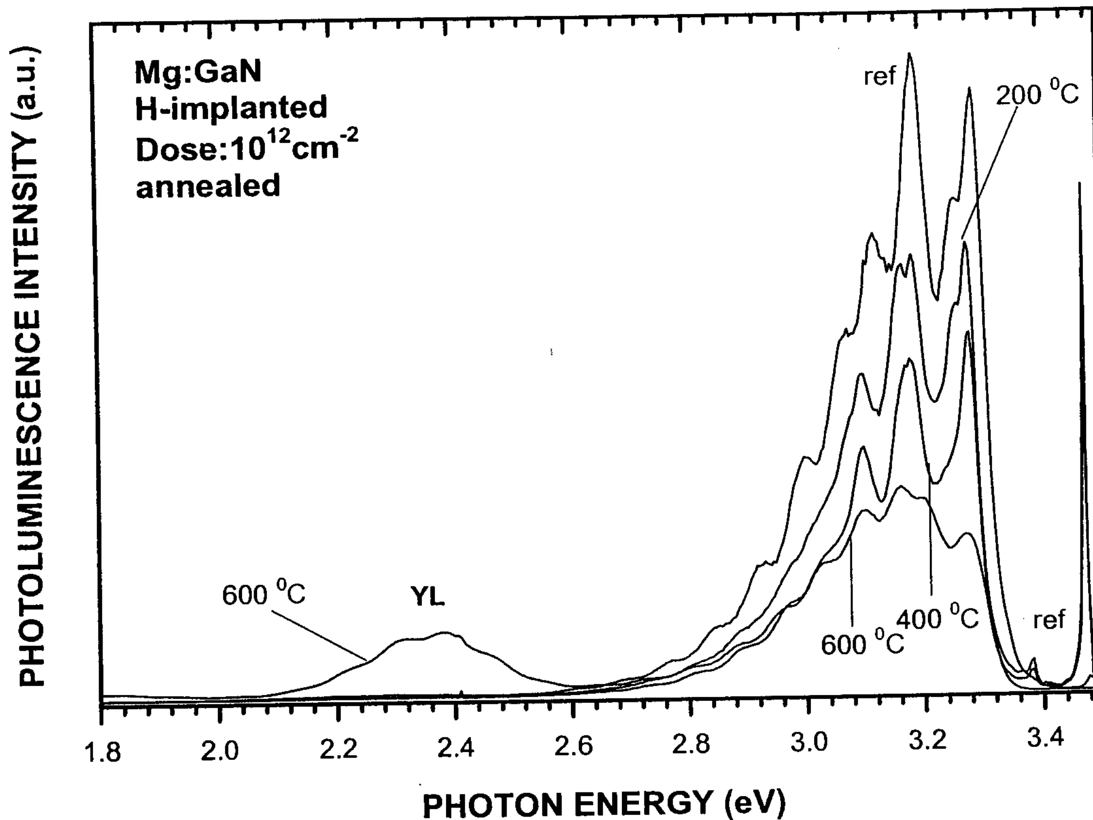

Figure 4.4. Photoluminescence spectra from Mg-doped GaN implanted with H at dose 10^{12} cm^{-2} and annealed.

The transition at 3.2eV is the highest in intensity since it involves the Mg doped impurities. The implantation and annealing (see figure 4.4) evidently induces an extremely sharp high-intensity transition at 3.473 eV, which is due to the recombination of excitons bound to neutral donors as well as a "new" excitonic band at 3.378 eV. In order to investigate these excitonic transitions (3.378 eV and 3.473 eV figure.4.5 we fitted a Lorentzian profile to the emission lines :

UNIVERSITEIT VAN PRETORIA
UNIVERSITY OF PRETORIA
YUNIBESITHI YA PRETORIA

$$I(E) = \sum_{i=1}^{2} \frac{2A_i}{\pi} \frac{\Gamma_i}{4(E - E_i)^2 - \Gamma_i^2} \qquad (4.1)$$

The fitted values are $E_1 = 3.475$eV, $E_2 = 3.481$eV, $\Gamma_1 = 2.4$ meV and $\Gamma_2 = 4.3$ meV. These results are consistent with previous measurements on these transitions. The 3.378 eV (figure 4. 5 and 4.6) emission line is close to the L_1 transiton found by Toth et al [4.8]. However, the authors did not discuss the detailed mechanism of its origin. The YL-line, centered at about 2.25 eV, is first observed after annealing at 600 °C.

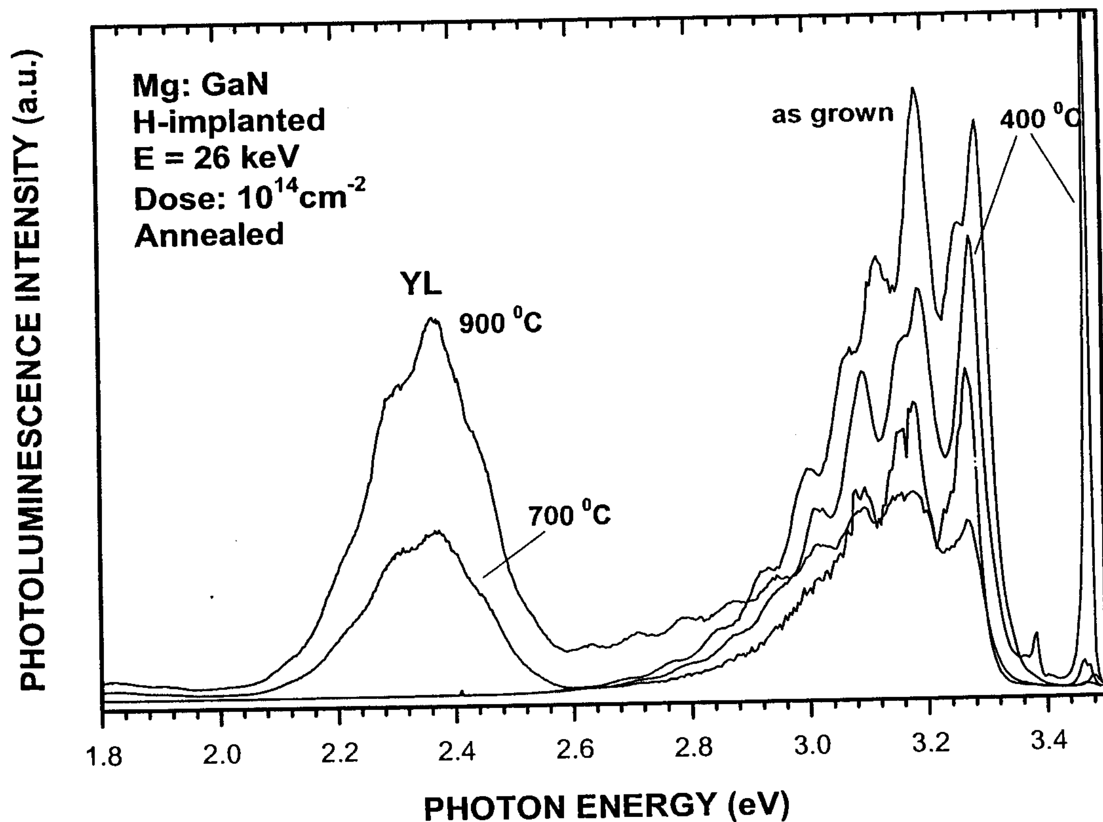

Figure 4.5. Photoluminescence spectra from Mg-doped GaN implanted with H at dose 10^{14} cm^{-2} and annealed.

Figure 4.5 shows the effect of higher implantation dose ($10^{14}cm^{-2}$) and higher annealing temperature. The induced YL band dominates the spectra while the DAP's bands are much lower in intensities and become structured. At very low implantation dose (10^{12} cm^{-2}) and annealing temperature (about 200°C) neither YL band nor new

excitonic transitions are observed. Instead, the DAP's bands become structured showing a number of phonon replicas. Figure 4.6 exhibits the DAP's with A_1(TO) 66 meV phonon replicas and figure 4.5 confirms the main mechanism for the YL band creation. At high implantation dose and low annealing temperature we do not observe the YL band. On the low energy side of the spectrum three sharp low intensities transitions are present.

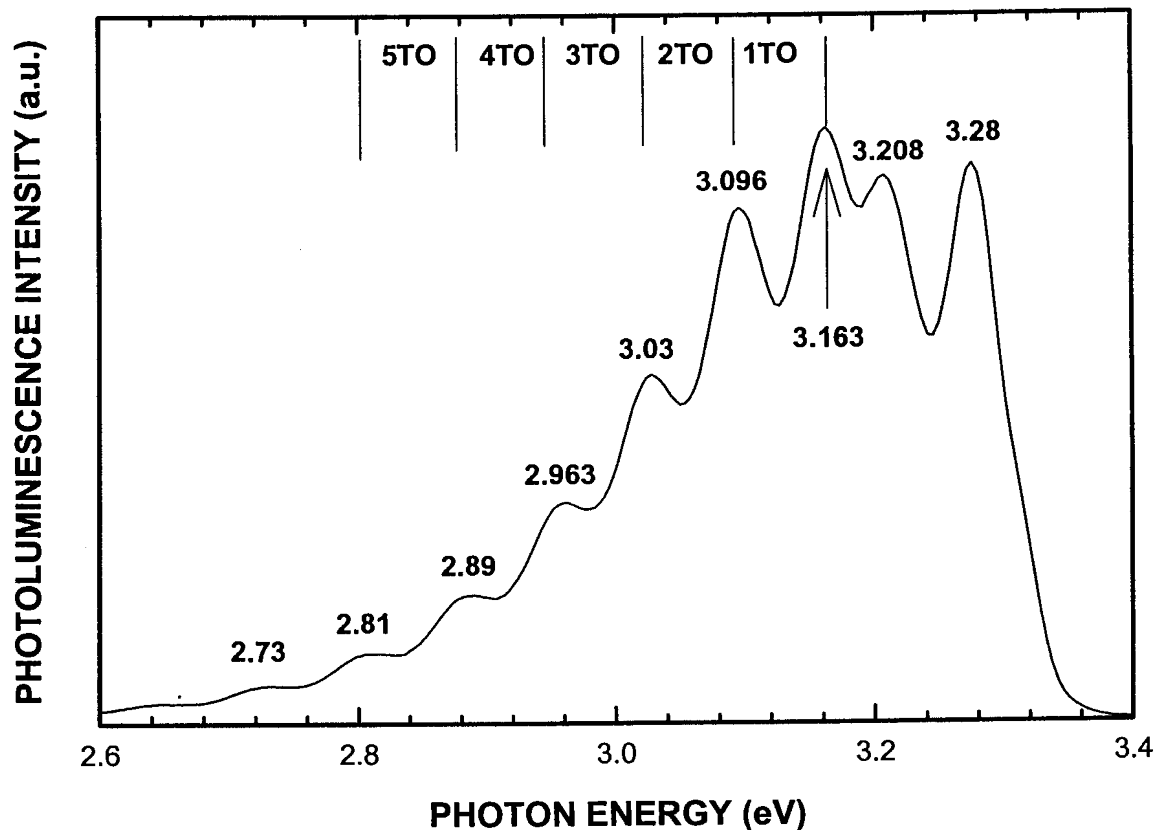

Figure 4.6. Phonon replicas monitored by photoluminescence spectroscopy.

A detailed recording of these lines is shown in figure 4.6 and 4.7. Their energy positions closely resemble the R_1 and R_2 transitions originating from Cr^{3+} ions in sapphire [4.9]. Their intensities are implantation dose dependent from which it can be inferred that the hydrogen ions might have reached the substrate and influenced Cr^{3+} aggregates. Trim profiles in figure 2.1 show hydrogen ions do not reach the sapphire. The maximum depth hydrogen ions can reach at 26 keV is approximately 400 nm. The hydrogen ions might have reached sapphire through channelling during implantation or diffusion. To check the hypothesis we have taken a Raman spectrum

(not shown) and the R_1 and R_2 transitions show up clearly at a "Raman shift" of 5006 and 5035 cm^{-1} corresponding to luminescence at the well known R_1 and R_2 wavelengths. The presence of Cr^{3+} ions in our sapphire substrate could be a result of hydrogen channelling or diffusion leading to Cr - H bond.

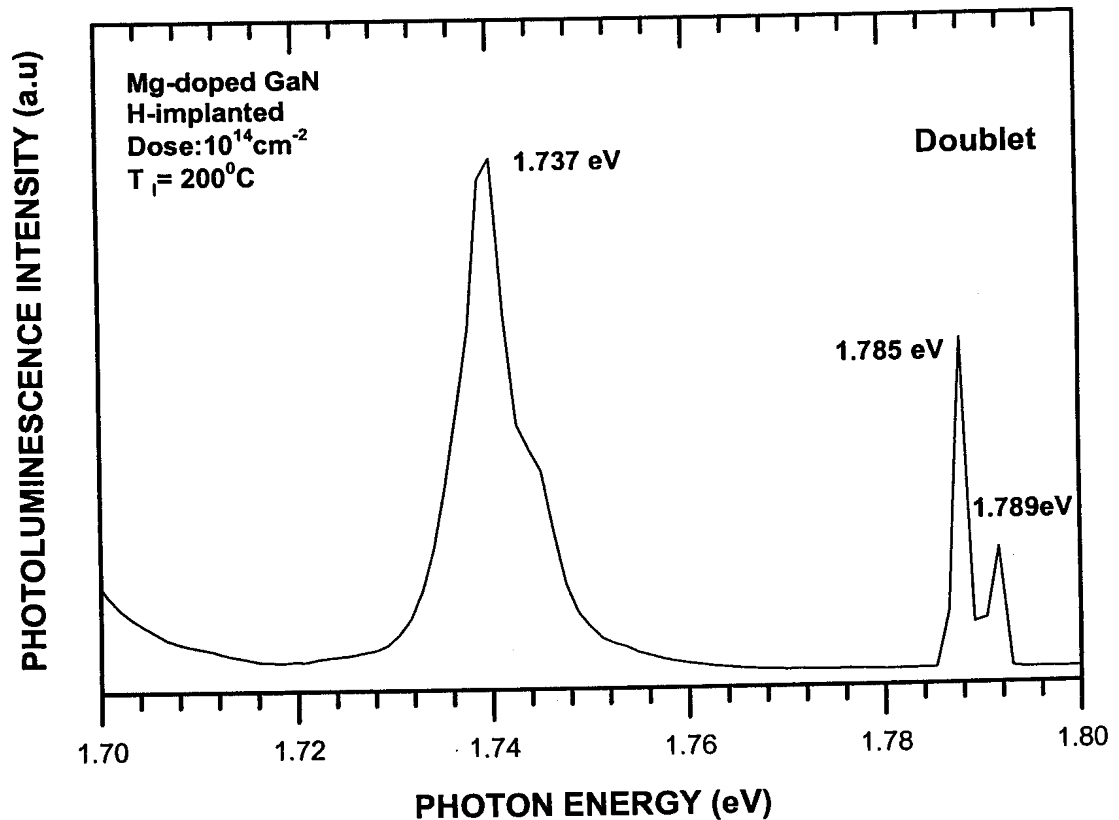

Figure 4.7.Enery positions of the R_1 and R_2 doublet observed by photoluminescence.

4.3. The yellow band

Figure 4.8 shows the plot of the intensity of the yellow band against annealing temperature for hydrogen-implanted Mg-doped GaN samples. In all samples the intensity of the yellow band tends to increase, reaches a maximum peak and decline with an increasing temperature. From the figure 4.8, it is clear that the yellow band seems to be depending on the annealing temperature, even though this dependency is not linear.

Another remarkable feature in figure 4.8 is the appearance of the yellow band in hydrogen-implanted samples. For sample implanted with 10^{15} cm^{-2} dose, the yellow band starts to emerge at 300^0C, whereas there is no trace of yellow band in other samples at this temperature. At 400 ^{0}C, the intensity for the yellow band is more prominent in this sample. However, at 600 ^{0}C the yellow band appears in all implanted samples as shown in figure 4.8 for each dose. The yellow band reaches maximum intensity at a specific temperature and drops rapidly at 900 ^{0}C. For 10^{12} cm^{-2}, 10^{13} cm^{-2} and 10^{15} cm^{-2} implanted samples, the maximum intensity is attained at 800 ^{0}C, 700 ^{0}C and 600 ^{0}C respectively.

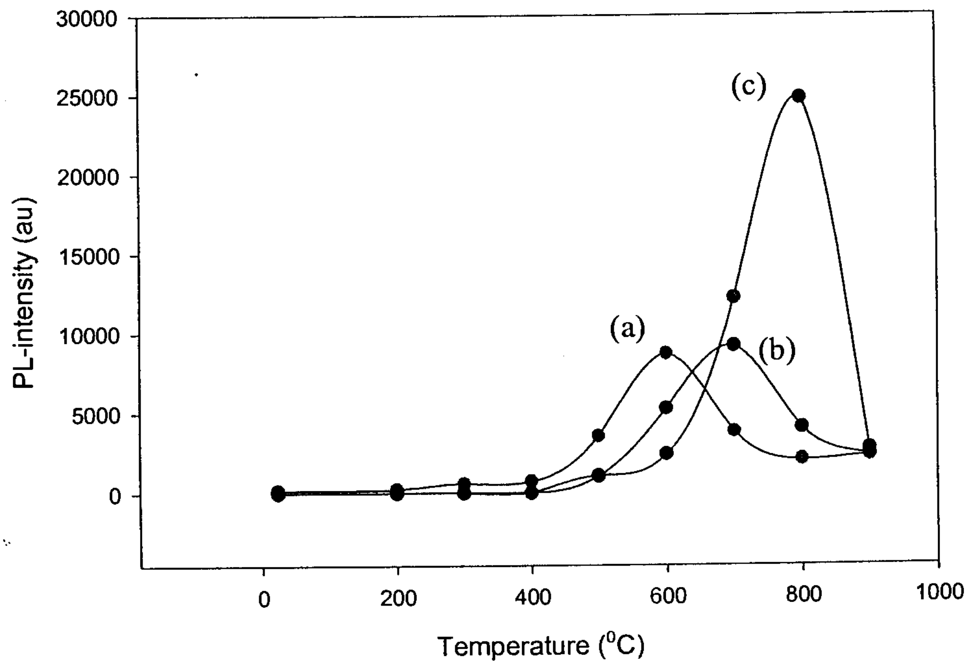

Figure 4.8. The PL-intensity of the yellow band plotted against temperature, the doses: (a) 10^{15} cm^{-2} (b) 10^{13} cm^{-2} (c) and 1x 10^{12} cm^{-2} (c).

4.4. The origin of the yellow band

It is important to understand what causes the yellow band and its origin because this yellow band if not understood, can interfere with the normal operation of the device. At this point it is important to explain briefly how the yellow band can be unprofitable in devices. Over and over again it is mentioned that the nitride semiconductors are potential candidates for the fabrication of the blue/ ultraviolet (UV) light emitting diodes or lasers because of their wide bandgap. The energy bandgap is the center of attraction for manufacturing of these devices. The presence of the yellow band can jeopardize the operation of such device in the form of emitting unwanted light due to some defects in the bandgap.

The origin of the yellow band is still a subject of speculations. Table 4.3 displays some of the speculations about the origin of the yellow band as observed in GaN materials.

Table 4.1. Some of the speculations on the origin of the yellow band.

Origin	type	Growth technique	reference
Transition from a deep donor state (E_v-0.8 eV) acceptor	n	MOVPE	[4.12]
Recombination process from a shallow donor deep level (E_v + 0.8 eV)	p	MBE	[4.13]
Shallow donor-deep acceptor transition	p	Regardless of growth technique	[4.11]
Native deep acceptor (V_{Ga})	n	calculation	[4.8]

The yellow band has been observed in heavy Mg-doped GaN [4.10]. It has been suggested that hydrogen behaves as a donor in p-type GaN and it forms complexes with acceptors. Annealing of the implanted samples activate hydrogen induced defects. But at low annealing temperatures (< 700^0C) there is no significant amount of redistribution of hydrogen 4.11], as a result the intensity of the yellow band increases. However, the intensity of yellow band decreased with an increasing temperature from

800^{0}C and above as shown figure 4.8. This decrease can be attributed to diffusion of hydrogen from the material [4.11].

This behaviour of the yellow band is observed in all implanted samples. This indicates that the yellow band in our work is directly linked to hydrogen-induced defects or it has to do with dissociation of the Mg-H complex in p-GaN because it is not observed in the spectrum of a control sample annealed at the same temperature.

UNIVERSITEIT VAN PRETORIA
UNIVERSITY OF PRETORIA
YUNIBESITHI YA PRETORIA

References

[4.1] M. Senthil Kumar, R Kesavamoorthy, P. Magudapathy, K. G. M. Nair and J. Kumar, I Nucl. Instr. And Meth. In Phys. Res. B **179** (2001).

[4.2] J. C. Nipko, C.K. Loong, C.M.N. Balkas, and R.F. Davis, Appl. Phys. Lett. **37**, 34 (1998).

[4.3] H. Harima, T. Inoue, S. Nakashima, M. Ishida, and M. Taneya, Appl. Phys. Lett. **75**, 1383 (1999).

[4.4] S. Murugkar, R. Merlin, A. Botchkarev, A. Salvador, and H. Morkoc, J. Appl. Phys. **77**, 6042 (1995).

[4.5] M. Pophristic, F. H. Long, M. Schurman, J. Ramer, I. T. Ferguson, phys. stat. sol. **216**, 803 (1999).

[4.6] B. Henderson, G. F. Imbusch, *in Optical Spectroscopy of Inorganic Solids*, Clarendon Press- Oxford, 1989.

[4.7] P. Perlin, T. Suski, H. Tesseyre, M. Leszczynski, I. Grzegory, J. Jun, S. Porowski, P. Boguslawski, J. Bernholc, J. C. Chervin, A. Polian, and T. D. Moustakas, Phys. Rev. Lett. **75**, 296, (1995).

[4.8] G. D. Chen, M. Smith, J. Y. Lin, H. X. Liang, M. Asif Khan, C. J. Sun, Appl. Phys. Lett. **67**, 1653 (1995).

[4.9] M. Toth, K. Fleischer, M. R. Philips, Phys. Rev B **59**, 1575 (1999).

[4.10] T. H. Maiman, R. H. Hoskins, I. J. D'Haenens, C. K. Asawa, and V. Evtuhov. Phys. Rev. **123**, 1151 (1961).

[4.11] J.Q. Duan B. R.Zhang, Y. X. Zhang, L.P. Wang, G. G. Qin, G. Y. Zahng, Y. Z. Tong, S. X. Jin, Z. J. Yang, X. Zhang, and Z. H. Xu, J. Appl. Phys. **82**, 5745 (1997).

[4.11] D. M. Hofmann, D. Kovalev, G. Steude, B. K. Meyer , A. Hoffmann, L. Eckey, R. Heitz , T. Detchprom , H. Amano, I. Akasaki , Phys. Rev. B **52**, 16702 (1995).

UNIVERSITEIT VAN PRETORIA
UNIVERSITY OF PRETORIA
YUNIBESITHI YA PRETORIA

[4.12] T. Monteiro, E. Pereira, M. R. Correia, C. Xavier, D. M. Hofmann, B. K. Meyer, S. ischer, A. Cremades, J. Piqueras, J.Lumin. 72, 696 (1997).

5. Conclusion

In this present study, the role of hydrogen in Mg-doped GaN was investigated. This was achieved by employing Raman spectroscopy and photoluminescence. Raman spectroscopy was employed to investigate changes in local vibrational mode as a result hydrogen implantation and the presence of Mg-H complexes in the p-type GaN.

Hydrogen ion implantation and annealing introduce several stable Raman modes of Mg-doped GaN. To our best knowledge we monitor for the first time by ordinary Raman spectroscopy the low energy acoustic phonon at 320 cm^{-1} (40 meV). Its symmetry assignment is given in the Appendix. The mode at 380 cm^{-1} is symmetry forbidden in any kind of GaN compound. It can be a feature of sapphire substrate or magnesium doping. The mode is the highest in intensity after the highest implantation dose and annealing temperature. The vibrational state 645 cm^{-1} is a Mg doping feature. But the new mode at 672 cm^{-1} evidently results from treatment. Several luminescence bands centred at about 1.8-1.88 eV in as grown and treated samples were found.

Two ruby fluorescence lines at 693 (R_1) and 694.4 nm (R_2) have been observed by PL and Raman spectroscopy. A comprehensive symmetry assignment of phonons belonging to the C^4_{6v} space group of GaN at **k** = 0 is given in the first Brillion zone.

At low hydrogen ion implantation dose and low annealing temperature a very sharp excitonic transition appears at 3.473 eV (as well as a band at 3.378 eV). The yellow band might be directly linked to hydrogen-induced defects or it has to do with dissociation of the Mg-H complex in p-GaN because it is not observed in the spectrum of a control sample annealed at the same temperature.

Appendix

a). The matrices of the D_{per} representation are obtained as follows:

$$E\begin{bmatrix} d_1 \\ d_2 \\ d_3 \\ d_4 \\ d_5 \\ d_6 \\ \alpha_1 \\ \alpha_2 \\ \alpha_3 \\ \alpha_4 \\ \alpha_5 \\ \alpha_6 \end{bmatrix} = (d_1, d_2, d_3, d_4, d_5, d_6, \alpha_1, \alpha_2, \alpha_3, \alpha_4, \alpha_5, \alpha_6)$$

$$A_1 = \begin{bmatrix} 1 & 0 & 0 & 0 & 0 & 0 \\ 0 & 1 & 0 & 0 & 0 & 0 \\ 0 & 0 & 1 & 0 & 0 & 0 \\ 0 & 0 & 0 & 1 & 0 & 0 \\ 0 & 0 & 0 & 0 & 1 & 0 \\ 0 & 0 & 0 & 0 & 0 & 1 \end{bmatrix}$$

$$D(E) = \begin{bmatrix} A_1 & 0 \\ 0 & A_1 \end{bmatrix}$$

$$\chi(E) = 12$$

$$(C_6/\tau)\begin{bmatrix} d_1 \\ d_2 \\ d_3 \\ d_4 \\ d_5 \\ d_6 \\ \alpha_1 \\ \alpha_2 \\ \alpha_3 \\ \alpha_4 \\ \alpha_5 \\ \alpha_6 \end{bmatrix} = (d_2, d_3, d_4, d_5, d_6, d_1, \alpha_2, \alpha_3, \alpha_4, \alpha_5, \alpha_6, \alpha_1)$$

$$A_2 = \begin{bmatrix} 0 & 1 & 0 & 0 & 0 & 0 \\ 0 & 0 & 1 & 0 & 0 & 0 \\ 0 & 0 & 0 & 1 & 0 & 0 \\ 0 & 0 & 0 & 0 & 1 & 0 \\ 0 & 0 & 0 & 0 & 0 & 1 \\ 1 & 0 & 0 & 0 & 0 & 0 \end{bmatrix}$$

$$D(C_6/\tau) = \begin{bmatrix} A_2 & 0 \\ 0 & A_2 \end{bmatrix}$$

$$\chi(C_6/\tau) = 0$$

$$C_3\begin{bmatrix} d_1 \\ d_2 \\ d_3 \\ d_4 \\ A_5 \\ d_6 \\ \alpha_1 \\ \alpha_2 \\ \alpha_3 \\ \alpha_4 \\ \alpha_5 \\ \alpha_6 \end{bmatrix} = (d_3, d_4, d_5, d_6, d_1, d_2, \alpha_3, \alpha_4, \alpha_5, \alpha_6, \alpha_1, \alpha_2)$$

$$A_3 = \begin{bmatrix} 0 & 0 & 1 & 0 & 0 & 0 \\ 0 & 0 & 0 & 1 & 0 & 0 \\ 0 & 0 & 0 & 0 & 1 & 0 \\ 0 & 0 & 0 & 0 & 0 & 1 \\ 1 & 0 & 0 & 0 & 0 & 0 \\ 0 & 1 & 0 & 0 & 0 & 0 \end{bmatrix}$$

$$D(C_3) = \begin{bmatrix} A_3 & 0 \\ 0 & A_3 \end{bmatrix}$$

$$\chi(C_3) = 0$$

$$(C_2/\tau)\begin{bmatrix} d_1 \\ d_2 \\ d_3 \\ d_4 \\ d_5 \\ d_6 \\ \alpha_1 \\ \alpha_2 \\ \alpha_3 \\ \alpha_4 \\ \alpha_5 \\ \alpha_6 \end{bmatrix} = (d_4, d_5, d_6, d_1, d_2, d_3, \alpha_4, \alpha_5, \alpha_6, \alpha_1, \alpha_2, \alpha_3)$$

$$A_4 = \begin{bmatrix} 0 & 0 & 0 & 1 & 0 & 0 \\ 0 & 0 & 0 & 0 & 1 & 0 \\ 0 & 0 & 0 & 0 & 0 & 1 \\ 1 & 0 & 0 & 0 & 0 & 0 \\ 0 & 1 & 0 & 0 & 0 & 0 \\ 0 & 0 & 1 & 0 & 0 & 0 \end{bmatrix}$$

$$D(C_2/\tau) = \begin{bmatrix} A_4 & 0 \\ 0 & A_4 \end{bmatrix}$$

$$\chi(C_2/\tau) = 0$$

$$\delta_v \begin{bmatrix} d_1 \\ d_2 \\ d_3 \\ d_4 \\ d_5 \\ d_6 \\ \alpha_1 \\ \alpha_2 \\ \alpha_3 \\ \alpha_4 \\ \alpha_5 \\ \alpha_6 \end{bmatrix} = (d_1, d_6, d_5, d_4, d_3, d_2, \alpha_1, \alpha_6, \alpha_5, \alpha_4, \alpha_3, \alpha_2)$$

$$A_5 = \begin{bmatrix} 1 & 0 & 0 & 0 & 0 & 0 \\ 0 & 0 & 0 & 0 & 0 & 1 \\ 0 & 0 & 0 & 0 & 1 & 0 \\ 0 & 0 & 0 & 1 & 0 & 0 \\ 0 & 0 & 1 & 0 & 0 & 0 \\ 0 & 1 & 0 & 0 & 0 & 0 \end{bmatrix}$$

$$D(\delta_v) = \begin{bmatrix} A_5 & 0 \\ 0 & A_5 \end{bmatrix}$$

$$\chi(\delta_v) = 4$$

$$\sigma_d / \tau \begin{bmatrix} d_1 \\ d_2 \\ d_3 \\ d_4 \\ d_5 \\ d_6 \\ \alpha_1 \\ \alpha_2 \\ \alpha_3 \\ \alpha_4 \\ \alpha_5 \\ \alpha_6 \end{bmatrix} = (d_2, d_1, d_6, d_5, d_4, d_3, \alpha_2, \alpha_1, \alpha_6, \alpha_5, \alpha_4, \alpha_3)$$

$$A_6 = \begin{bmatrix} 0 & 1 & 0 & 0 & 0 & 0 \\ 1 & 0 & 0 & 0 & 0 & 0 \\ 0 & 0 & 0 & 0 & 0 & 1 \\ 0 & 0 & 0 & 0 & 1 & 0 \\ 0 & 0 & 0 & 1 & 0 & 0 \\ 0 & 0 & 1 & 0 & 0 & 0 \end{bmatrix}$$

$$D(\sigma_d / \tau) = \begin{bmatrix} A_6 & 0 \\ 0 & A_6 \end{bmatrix}$$

$$\chi(\sigma_d / \tau) = 0$$

b.) **The Raman active modes are contained in the symmetrized KP of the vector representation $D^v = A_1 + E_2$**

The active modes are found by means of the reduction formula

$$\mu_{ri} = \frac{1}{g}\sum \chi^D (g/\tau_g).\chi^{ri(*)} (g/\tau_g).g_i$$

where μ_{ri} represents A_1, A_2, B_1, B_2, E_1, and E_2.

Using table 3.1 of characters, we find:

$$[A_1 \oplus E_2]^{sym}_{(2)} = 2A_1 \oplus 2E_1 \oplus 2E_2$$

Therefore, the vibrational modes of GaN observed by Raman spectroscopy are: A_1 (TO), A_1 (LO), E_1(TO), E_1(LO) E_2,(low) and E_2 (high). Most of these modes are present in our spectra (see figure 4.1a and 4.1b).